

Article

Application of Parameterized Grain-Size Endmember Modeling in the Study of Quaternary Oxbow Lake Sedimentation: A Case Study of Tövises Bed Sediments in the Eastern Great Hungarian Plain

Abdelrhim Eltjani , Dávid Molnár , László Makó, János Geiger and Pál Sümegi

Department of Geology and Paleontology, University of Szeged, H-6722 Szeged, Hungary

* Correspondence: molnard@geo.u-szeged.hu

Abstract: Abandoned channels are essential in the Quaternary floodplains, and their infill contains different paleoenvironment recorders. Grain-size distribution (GSD) is one proxy that helps characterize the alluviation and associated sedimentological processes of the abandoned channels. The classic statistical methods of the grain-size analysis provide insufficient information on the whole distribution; this necessitates a more comprehensive approach. Grain-size endmember modeling (EMM) is one approach beyond the traditional procedures that helps unmix the GSDs. This study describes the changes in the depositional process by unmixing the GSDs of a Holocene abandoned channel through parameterized EMM integrated with lithofacies, age–depth model, loss-on-ignition (LOI), and magnetic susceptibility (MS). This approach effectively enabled the quantification and characterization of up to four endmembers (EM1–4); the characteristics of grain-size endmembers imply changes in sedimentary environments since 8000 BP. EM1 is mainly clay and very fine silt, representing the fine component of the distribution corresponding to the background of quiet water sedimentation of the lacustrine phase. EM2 and EM3 are the intermediate components representing the distal overbank deposits of the flood. EM4 is dominated by coarse silt and very fine sand, representing deposition of overbank flow during the flood periods. This paper demonstrates that the parametrized grain-size EMM is reasonable in characterizing abandoned channel infill sedimentary depositional and sedimentation history.

Keywords: grain-size endmembers; oxbow lake; Holocene; paleohydrology; Great Hungarian Plain



Citation: Eltjani, A.; Molnár, D.; Makó, L.; Geiger, J.; Sümegi, P. Application of Parameterized Grain-Size Endmember Modeling in the Study of Quaternary Oxbow Lake Sedimentation: A Case Study of Tövises Bed Sediments in the Eastern Great Hungarian Plain. *Quaternary* **2022**, *5*, 44. <https://doi.org/10.3390/quat5040044>

Academic Editors: Marcello Tropeano and Henry Lamb

Received: 13 July 2022

Accepted: 18 October 2022

Published: 25 October 2022

Publisher's Note: MDPI stays neutral with regard to jurisdictional claims in published maps and institutional affiliations.



Copyright: © 2022 by the authors. Licensee MDPI, Basel, Switzerland. This article is an open access article distributed under the terms and conditions of the Creative Commons Attribution (CC BY) license (<https://creativecommons.org/licenses/by/4.0/>).

1. Introduction

Grain-size distribution (GSD) is a fundamental aspect of sediments and is widely utilized to characterize different sediment transport processes. Fluvial transport is an essential transporting mechanism; the deposits of a fluvial channel are either accumulated through the channel or by infilling an abandoned channel. Abandoned channel fills are common in Quaternary fluvial systems; they result from complex meander migration over the floodplain [1]. Three distinct stages can be described: cutoff initiation, plug bar formation, and channel disconnection [2]. The cutoff occurs when the discharge flows through the new channel and does not reach the meander loop [2–4]; as a result, plug bar sediments accumulate, further triggering blockage of the discharge [5], and the meander loop becomes a floodplain lake [2]. Channel-fill sediments contain proxies that can be used for paleoenvironmental reconstructions [2]. GSD of these infills is one of the paleoenvironmental proxies that help characterize the alluviation history of the abandoned channels. Fluvial sediments exhibit polymodal GSD [6], comprising many overlapping subpopulations [3,4] corresponding to different transport mechanisms and depositional processes [6]. Deciphering the depositional conditions from such distribution requires a thorough understanding of the individual components, which cannot be achieved by

the classic statistical analysis (e.g., graphical descriptive method and statistical methods of quartile measures and method of moments). In recent years, grain-size EMM has become common in grain-size analysis [7–9] for unmixing the GSDs, unveiling the obscured information on the sedimentation process, and helping reconstruct paleoenvironments and the infill history of oxbow lakes. The grain-size endmembers (EMs) are obtained by statistically unmixing robust sub-populations, with each endmember representing a proportion of particles deposited by the same sedimentary processes [10]. EMM was applied to reconstruct sediment sources and sedimentation processes in various sedimentary environments—marine [11–14], aeolian [9,15,16], lacustrine [10,17–20], and fluvial [21,22]—employing different unmixing algorithms and producing promising results. Later on, in Quaternary sediments, the application of EMM has been promising, albeit it has not been extensively employed to study Quaternary abandoned channel sediments and is more often applied in the marine realm. After the first unmixing algorithm was published by Weltje [23], many investigators have developed new unmixing algorithms, e.g., EMMA-geo [24], AnalySize [25], BEMMA [26], and BasEMMA [27]. Since oxbow lakes function as a sediment sink during floods with high preservation potential, and their sediments offer an excellent proxy concerning polymodality of the GSDs, thus providing essential information regarding depositional processes and dynamics, EMM can help reconstruct paleoenvironments and the infill history of oxbow lakes.

Extensive studies of Quaternary paleoenvironmental reconstructions have already been conducted in the Great Hungarian Plain (GHP); for instance, [28–31]. Still, information on the Quaternary channel fill sediments is limited; many more records are required to fully document the spatiotemporal patterns of past environmental and depositional processes across the GHP. This paper intends to show that the abandoned channel-fill sequences are useful recorders of sedimentological processes and paleofloods by improving the understanding of the internal build-up of the oxbow lake sedimentary sequence through grain-size EMM. This study investigates the sediments of the Tövis channel, a Quaternary oxbow lake near Pocsaj in the eastern GHP (Figure 1). The topmost Holocene sequence of the study area and its vicinity is made up of loess sequences overlain by alluvial fan sediments [32,33].

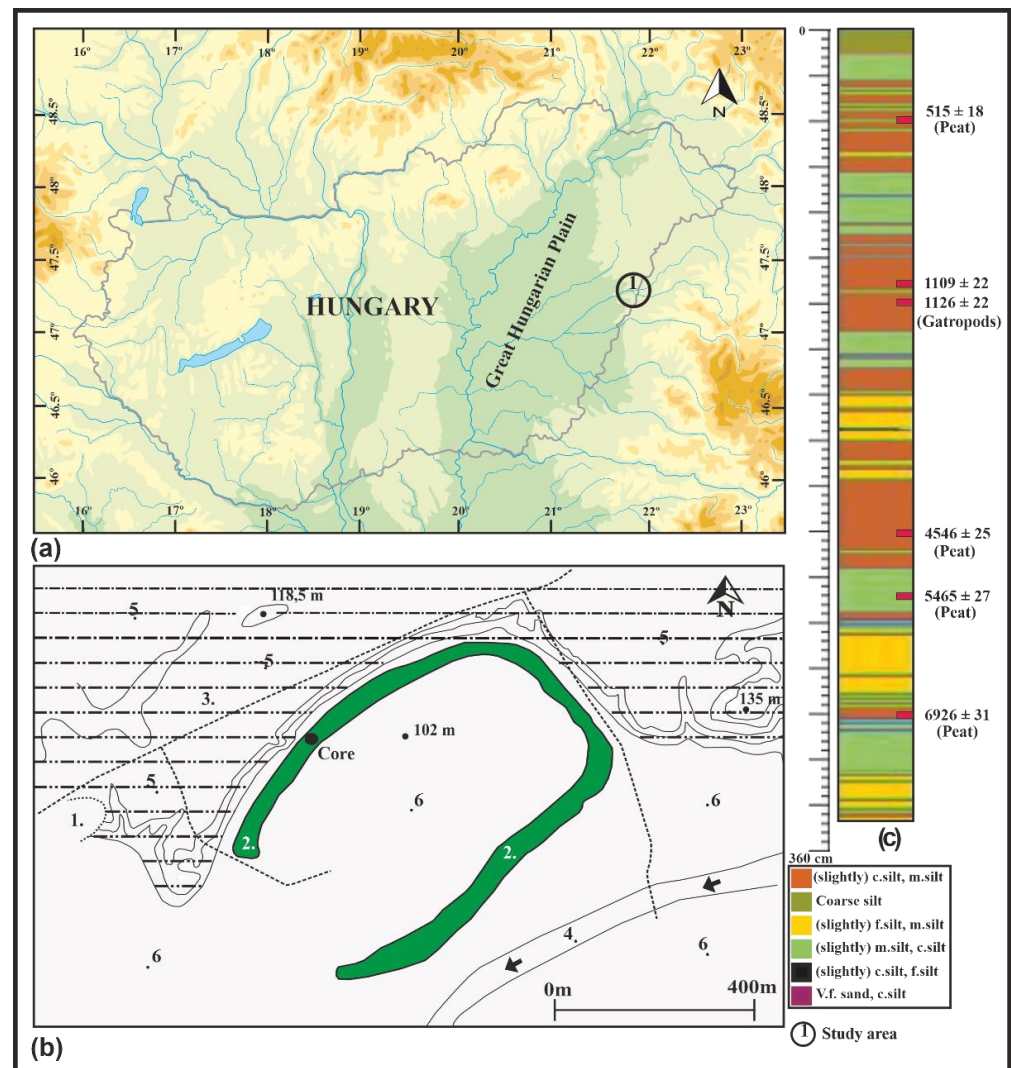


Figure 1. Map of the study area. (a) Location of the Tövises bed paleochannel in GHP; (b) the core location within Tövises bed paleochannel and geology of the vicinity: 1. sandpit, 2. Tövises bed paleochannel, 3. loess-covered Pleistocene alluvial fan, 4. canalized bed of Ér creek, 5. loess, and 6. alluvia sediments; (c) lithology profile of the core.

2. Materials and Methods

2.1. Lithology and Geochronology

A 346 cm long undisturbed sediment core was retrieved using a 5 cm diameter sealed liner tube Russian peat corer. The analysis routine and sample treatment are based on [34]. The samples were dried at 55 °C. Then, 30 mL of $\text{Na}_2\text{P}_6\text{O}_{18}$ solution was added to 0.6 g of the sample and treated in an ultrasonic bath to disperse the particles. The ^{14}C chronology was based on AMS dates from six samples analyzed at the International Radiocarbon AMS Competence and Training Center (INTERACT), Institute for Nuclear Research, Loránd Eötvös Research Network, Debrecen, Hungary. The radiocarbon dates were calibrated to calendar ages in CALIB 8.1 using the IntCal20 calibration curve. The age–depth modeling was performed in R language version 4.1.3 using the R bacon 2.5.8 age–depth modeling package [35] and was based on Bayesian statistics.

2.2. Grain-Size Analysis and Endmember Modeling (EMM)

GSDs of the pretreated sediment core samples were obtained at one cm intervals for 42 grain-size classes ranging from 0.1 to 500 μm by laser diffraction using the Easysizer20 laser particle analyzer (OMEC) available at the Geoarchaeological and Palaeoecological

Lab of the Department of Geology and Paleontology, University of Szeged, Hungary. The instrument has a measuring range of 0.1 to 500 μm and a repeatability error of less than 3%. The device uses 54 built-in detectors based on the Mie scattering. The grain-size scale and nomenclature used here are based on the Wentworth scale [36]. The unmixing of the measured GSDs was performed using the AnalySize v.1.2.0 EMM algorithm [25], a freely available MATLAB-based graphic user interface (GUI) software. The algorithm transforms the original distribution into unimodal endmembers (EMs) [10], and the optimum number of the EMs is determined based on the coefficient of determination (R^2) and the angular deviation (θ) between the endmembers and the GSDs. This procedure produces accurate fitting results and helps avert data over-fitting [9]. The Weibull function can provide an accurate explanation of the dynamicity of the EMs sedimentation process when decomposing the GSD by considering the geological background of the GSD, resulting in a greater statistical and physical significance of the EMM [9]. The parameterization method used is the General Weibull Distribution function [37].

2.3. Loss-On-Ignition (LOI) and Magnetic Susceptibility (MS)

The sediment (LOI) parameters of this study, i.e., organic material (OM) and carbonate content, were measured at 1 cm resolution following the general LOI procedure [38,39]. One gram of each sample was subject to sequential heating for 24 h at 550 $^{\circ}\text{C}$ to combust the (OM) (LOI_{550}) and at 950 $^{\circ}\text{C}$ to evacuate the CaCO_3 from carbonate content (LOI_{950}) and the measured parameter expressed in weight percent.

MS is a bulk measurement representing the sum of all the individual susceptibility contributions from the different magnetic mineral grains in the sediment sample. Therefore, it indicates the composition changes linked to paleoclimatic conditions that control sedimentation processes by measuring magnetizable sediment contents. In this study, the MS is measured for homogenous bulk samples using the Bartington MS2 Meter at a 2.7 MHz frequency [40]; each sample was measured three times, and the obtained values were averaged. We used the cumulative sum (CUSUM) chart to monitor and detect small shifts and change points in the magnetic susceptibility values. CUSUM uses the cumulative sum of deviations from a given data or subgroup means, and this method is sensitive to small shifts in the process mean [41].

3. Results

3.1. Lithology and Stratigraphic Divisions

The ^{14}C ages of the Tövises bed core range from 7748 BP at 304 cm to 532 BP at 43 cm (Table 1) (Figure 2a).

Table 1. AMS radiocarbon dates for samples from Tövises bed core.

Lab ID	Depth (cm)	Sample Type	Conventional ^{14}C Age	Calibrated ^{14}C Age (2σ BP)	Weighted Mean ^{14}C Age (BP)
DeA-29986	43	Peat "bulk"	515 \pm 18	514–545	532 \pm 15.5
DeA-29550	116	<i>P.corneus</i> shell	1109 \pm 22	958–1058	1007 \pm 50
DeA-29551	121	<i>P.corneus</i> shell	1126 \pm 22	959–1065	1016 \pm 53
DeA-29988	224	Peat "bulk"	4546 \pm 25	5052–5188	5161 \pm 68
DeA-29990	252	Peat "bulk"	5465 \pm 27	6266–6305	6273 \pm 19.5
DeA-29992	305	Peat "bulk"	6926 \pm 31	7678–7799	7748 \pm 60.5

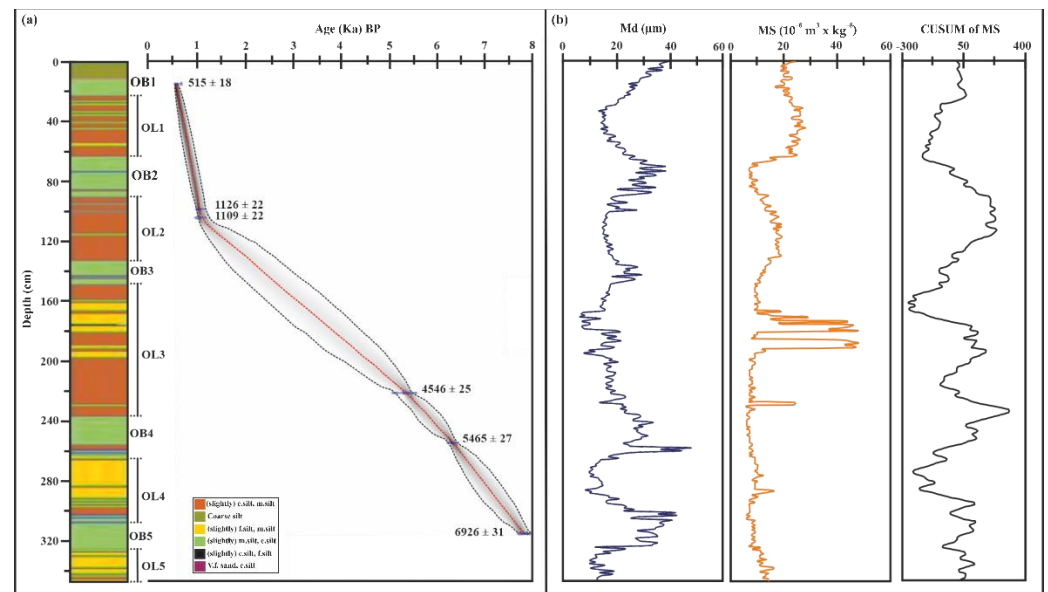


Figure 2. Stratigraphic division of the Tövises bed sequence. (a) Age–depth model, the calibrated ^{14}C dates (blue, with 2σ errors), and darker grey shading represent the probable calendar ages; grey stippled lines indicate 95% confidence intervals; the red line is the single “best” model based on the weighted mean ages. (b) MS, the median grain size (Md) and the CUSUM curve of the MS. We use the notation OL to represent the oxbow lake facies-dominated phase and OB for the overbank lithofacies-dominated phase. The depth scale is shared between the (a,b) panels.

Details of the radiocarbon ages used to construct the age–depth models are shown in Table 1. The Bacon-built age–depth model (Figure 2a) is concurrent ($R^2 = 0.99$) for the 7748 years represented by the Tövises bed sediments. Between circa 8000 and 6000 BP, the predominant sediments accumulated are fine and medium silts intercalated coarse silt, with a minor fine sand fraction. Following a transition between approximately circa 6000 and 2500 BP, the sediment changed to the dominant sediments containing medium and coarse silts with fine silt, which was less dominant. Between circa 2500 and 500 BP, the dominant sediment composition remained relatively unchanged (i.e., medium and coarse silt): fine and medium silt intercalated coarse silt with a minor, very fine sand fraction. Accumulation of the coarse silt continued until the channel became abundant.

Based on the ^{14}C data age–depth model and lithofacies data (Table 2) combined with the variation MS curve, cumulative sum (CUSUM) curve of MS, and median particle size (Md), the vertical subdivision of the Tövises bed sequence was conducted (Figure 2). The identified units represent identical floodplain environments with associated processes: abandoned channel, oxbow lake phase frequently intercalated with flood deposits. The bottom base sequence of circa 7500–6700 BP represents the oxbow infill sequence characterized by massive silt clay facies interbedded and overlaid with lacustrine gyttja of the coarse silt to clay organic-rich facies, which represent significant flood events. Intervals circa 2700–2000 BP and circa 500–0 BP are massive, rooted clay silt facies with downward decreasing root intensity representing distal overbank soil. The presence of plant wood debris, oxidized brown spots, and abundant shells characterizes the layers at circa 2000–1000 BP and circa 850–500, with decreasing shell content towards the bottom; this layer represents lacustrine gyttja resulting from the infill of the abandoned channel. At the depth from circa 6700–5800 BP, the layer combines lacustrine gyttja and wetland histosol (peats) and is part of an interrupted oxbow lake infill phase. On many occasions, the massive organic-rich deposits (gyttjas) contain terrestrial gastropods and brachiopod shells with abundant wood fragments. A wetland histosol sequence is characterized by peat facies (O) of varied thicknesses.

Table 2. The lithofacies association encountered in the Tövises bed core, described following Hicks and Evans [42].

Lithofacies	Texture and Structures	Interpretations
Silt (SSm)	Massive silt, coarse-grained	Distal overbank
Mud (MI)	Laminated silt and clay	Oxbow lake flood layer
Mud (Mmo)	Massive silt, clay, OM	Oxbow lake infill
Mud (Mmr)	Massive silt and clay (rooted soil)	Distal overbank (soil)
Peat (O)	Massive peat, fibrous	Wetland histosol
Sand (Smf)	Massive, very fine-grained	Proximal overbank
Sand (Smo)	Massive (wood remains), very fine-grained	Proximal overbank

3.2. Grain-Size Distribution (GSD) and Endmember Modeling (EMM)

3.2.1. Grain-Size Distribution (GSD)

The GSDs of the sediments in the Tövises bed core consist of clay (<8 Φ), silt (8 to 4 Φ) with dominant values from 4.3 Φ to 5.2 Φ, and very fine sand (>4 to 3 Φ) (Figure 2a). The silt content represents the dominant fraction with a content of 80.7%. The samples contained less clay (13%). The sand fraction represents the least dominant fraction and has a content of 6% (Figure 3b).

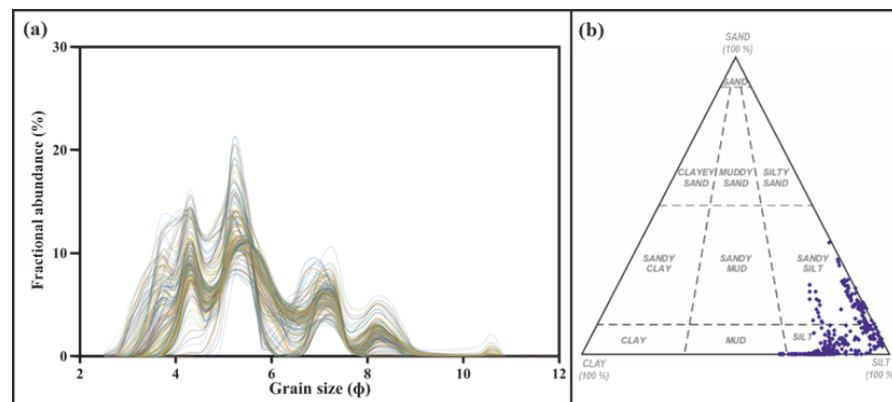


Figure 3. GSD characteristics of the Tövises bed core. (a) Overlay plot of the GSDs of all samples ($n = 345$), illustrating the polymodality of Tövises bed core sediments; (b) classification of grain-size composition in Tövises bed core, fine ternary plot [43].

3.2.2. Endmember Modeling (EMM)

All the sediment samples collected from the core were subjected to EMM. The GSD analysis revealed several polymodal distributions ranging from 2.5 to 11 Φ (Figure 4b). The samples were predominantly silt, with mean grain sizes fluctuating with depth. The optimum number of EMs was determined based on the inflection point of the determination coefficients (R^2) plot [25] (Figure 4a). The four EMs model is the turning point in linear correlations (Figure 4a). The good of fit statistics demonstrates that these four endmembers offer great optimization of the grain-size subpopulations and R^2 (94% of the total variance); thus, the four EMs model meets the need for the least EM number with a high R^2 . Figure 4b indicates the grain-size distribution of the selected EMs. Table 3 shows the endmember statistics; EM1 is characterized by moderately to well-sorted, fine skewed distribution between clay and very fine silt with a mean grain size of 7.45 Φ. EM2 and EM3 are well to very well sorted, finely skewed coarse to fine silt with mean grain sizes 5.5 and 6.1 Φ, respectively. EM4 is moderately sorted, finely skewed, and very fine sand to medium silt with a mean grain size of 4.65 Φ. The proportional contributions of each endmember are 26.43% for EM1, 12.21% for EM2, 18.90% for EM3, and 42.46% for EM4.

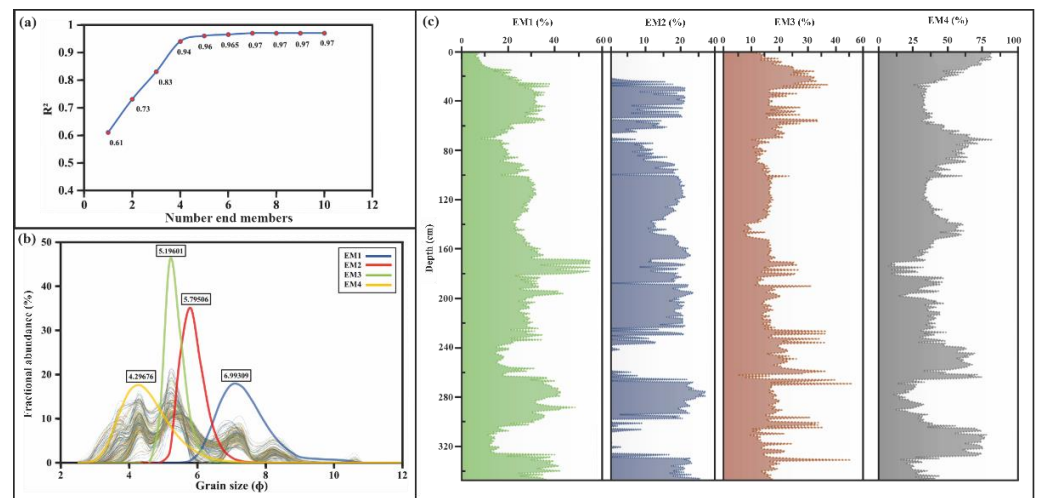


Figure 4. EMM results of sediments from the Tövises bed core. (a) The multiple coefficients of determination (R^2) function of the number of Ems. (b) Representative four EMs resulting from modeling. (c) The vertical distribution of the four EMs abundance of Tövises bed core.

Table 3. The statistical parameters of EMs of the Tövises bed core sediments.

EM	Mean Grain Size (Mz)	Sorting (σ)	Skewness (Sk)	Kurtosis (Kg)	Clay (%)	Silt (%)	Sand (%)
EM1	7.45	0.70	0.13	1.00	21.50	78.50	0.00
EM2	6.00	0.37	0.16	1.00	0.03	99.97	0.00
EM3	5.50	0.29	0.18	1.00	0.00	100.00	0.00
EM4	4.70	0.72	0.17	1.00	0.00	83.00	17.00

The mean grain size (Mz) relates to the overall grain size. The average sediment size is Mz, representing the index of depositional energy conditions; it exhibits local variations within the sediment core, ranging from silt to very fine sands; this variation in the Mz indicates fluctuations in the depositional energy. The correlation analysis shows a positive correlation between Mz and EM4; therefore, EM4 can indicate the energy conditions of the deposition. The average EM4 of the Tövises bed sediments in the area points to the predominance of coarse silt, indicating a moderately low energy deposition condition. The endmember distributions in each identified layer of the Tövises bed core are calculated, and the results are presented in (Figure 5). The variation trend of average EM1 content is equal in all oxbow lake infill units (OL1–OL5) and higher than its content in all overbank units (OB1–OB5). EM2 and EM3's average content fluctuates in all units and appears equal for OL2 and OL5; on the other hand, EM2 is present in OB4 and OB5. The EM4 is present in all units, and its average contents in all overbank units (OB1–OB5) are higher than in the oxbow lake infill units.

3.3. Loss-On-Ignition (LOI) and Magnetic Susceptibility (MS) Characteristics

The LOI record obtained from the core sediments shows distinct shifts in organic content that mark the different oxbow filling phases (Figure 2a), with fluctuations within the oxbow lake infill facies-dominated phases associated with a gradual transition in sediment grain sizes.

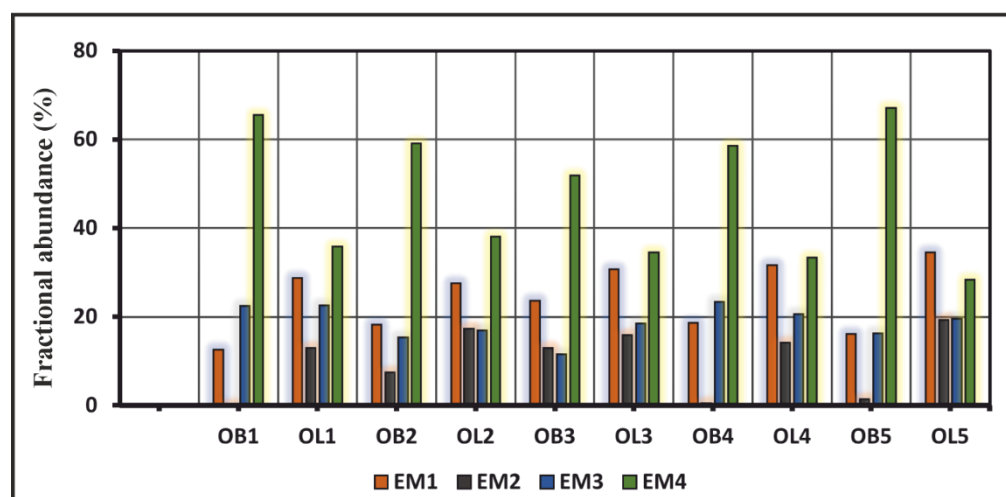


Figure 5. Average of endmembers abundance (EM1-4) of each core unit.

In the Tövises bed sediments, the lower MS values range from 6×10^{-8} to $10 \times 10^{-8} \text{ m}^3 \times \text{kg}^{-1}$, with an average value of $8 \times 10^{-8} \text{ m}^3 \times \text{kg}^{-1}$, while the high MS ranges from 27 to $48 \times 10^{-8} \text{ m}^3 \times \text{kg}^{-1}$. The higher range of MS shows three distinct and prominent peaks; on the other hand, the low range exhibits fluctuation of increasing and decreasing trends (Figure 2b). The MS values change points at different intervals, and they are conformable with Md trends (Figure 2a,b); the highest value (48×10^{-8}) is between circa 3000 and 400 BP and between circa 3000 and 1700 BP, the value ranges (5 to $19 \times 10^{-8} \text{ m}^3 \times \text{kg}^{-1}$) and (4 to $14 \times 10^{-8} \text{ m}^3 \times \text{kg}^{-1}$) at circa 1700–1000 BP, and the values at circa 400–1000 BP ranges (19 to $23 \times 10^{-8} \text{ m}^3 \times \text{kg}^{-1}$).

4. Discussion

After cutting off from the main channel, the oxbow lake receives water and sediment delivered by a tie channel and overbank flow. The abandonment process starts with cutoff initiation, where the channel is separated from the meander loop and flows a new straight course; as the channel diverts, the plug bar forms, causing further blockage of the upper and lower junction of the oxbow lake [3–5]. The regular channel discharge does not reach the developing abandoned channel [2]. Suspended sediment accounts for most sediment loads in most river systems [44,45]. The subsequent high discharge removes the sediments deposited during the previous low discharge [46].

The analyzed data show that the Tövises bed paleochannel evolved during the mid to late Holocene around 7748 ± 60 – 532 ± 15 BP, through an early lacustrine phase (oxbow lake) gradually infilled by lacustrine gyttjas, interbedded with wetland histosol, and periodically accumulating flood deposits. The lithofacies succession (Table 2) indicates different depositional settings and transport mechanisms. The overbank sequence of alternating dark layers of coarse silt and very fine sand represents flood sediments followed by finer sediment settling out of suspension after floods, respectively [47]. The organic-rich beds are likely to indicate the exposure of infill sediments to wetting and drought cycles which were probably part of the changing Holocene climate across Europe, where the different magnitude of changes was scattered in the content. For instance, during the mid-Holocene, Europe experienced the wettest period where the precipitation was about 20 mm/year higher than the current. Around circa 8000 BP, warm and dry conditions were prevailing in central Europe, with small-scale changes in temperature [48], while in the east cold and wet conditions were present; during the late Holocene, the climatic conditions were cold and wet in central Europe [49] and northern Europe [48] and warm and dry in eastern Europe [49].

The presence of peat indicates the accumulation of terrestrial organics [43]. The peat-forming conditions are favored by preventing flood water accessibility to the accumulation

site and mixing with clastic sediments [50]; warm and moist conditions are closely correlated with hydrologic factors [50]. However, the peat contains clastic sediments and is often intercalated with thin overbank facies indicating the lake transition into wetlands, probably caused by changes in lake and main channel connectivity [51]. The peat layers at depths of 43, 224, 251, and 305 cm (Figure 2a) indicate consistent development of organic-rich sediments over a prolonged period. Moreover, peat layers between oxbow infill imply recurring drying up and reactivation of the oxbow lake. The fluctuations in organic content within the oxbow lake infill's facies-dominated phases are interpreted as sudden changes in the active channel vicinity due to abrupt migration through revived cutoffs in the main channel. The transition in sediment grain sizes within phases probably represents a gradual change in connectivity and lateral river migration. The high superimposed small-scale values probably reflect sedimentation during minor to moderate and more significant floods, peat formation, inter-flood organic production, and other soil-forming processes.

The EMM of the GSDs of the last 8000 BP of the Tövises channel reveals valuable and independent information on the evolution and its alluviation process in the temperate mid-latitude GHP. The GSDs were separated into statistically robust EMs, each representing a distinct particle population assumed to be transported and deposited by a particular sedimentation process. Most of the suspension load in rivers originates outside the river channel and is delivered as overland flow; it can also originate from riverbank erosion [45]. EM1 is predominantly clay to very fine silt and relates to background fine sediments within the oxbow lake that occur irrespective of the river phase. Silt-sized particles are transported primarily as a suspended load, while sandy fractions are transported as a bedload, i.e., by traction or saltation [52]; the higher abundance of EM1 and EM2 is associated with the oxbow lake infill phase (OL1-5). In addition, the high MS values associated with EM1-2 and OL1-5 (Figures 2 and 6) indicate wet and reducing periods followed by drier periods resembling lacustrine conditions that are periodically exposed to dry seasons. MS reflects the mineral contents of the sediments; ferrimagnetic minerals contribute the most to the MS in the sediments, however, besides iron-rich clay minerals [53]. MS is higher in the sediments and soils than in the parent rocks and topsoil than in the sub-soils [53,54]. It results from the in situ alterations of the iron oxides from an antiferromagnetic form to the ferromagnetic form; this alteration requires wet conditions [55]. During wet conditions, the anaerobic breakdown of soil organic matter leads to the reduction of iron; during the subsequent dry period, the iron is re-oxidized to form maghemite [54]. The intermediate components, EM2 and EM3, are mainly silt and are probably deposited during low to moderate flooding events.

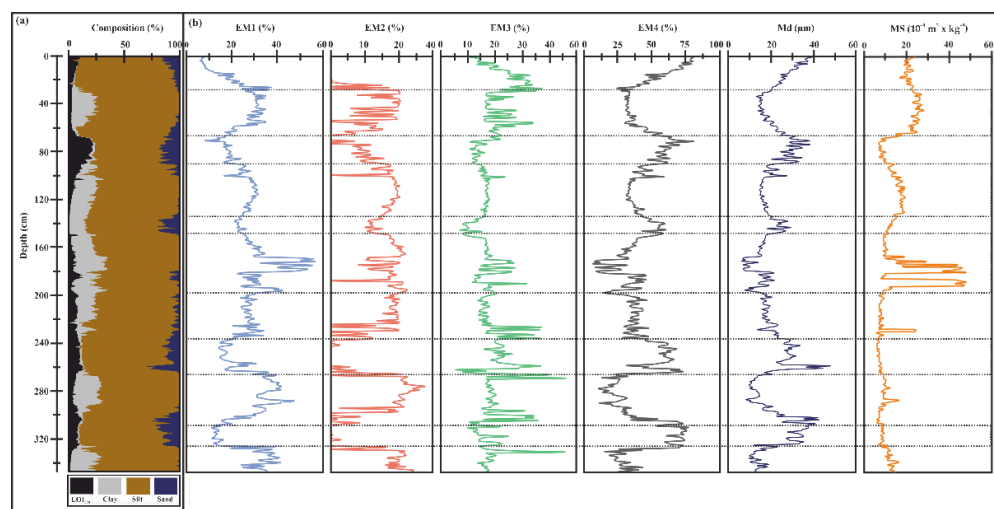


Figure 6. Sedimentary characteristics of the Tövises bed core. (a) Grain-size composition and LOI data. (b) Grain-size endmembers (EM1–4), magnetic susceptibility, and median particle size (Md) curves. The depth scale is shared between the (a,b) panels.

The coarsest component, EM4, is coarse silt to very fine sand that is interpreted as coarse sediments entrained in suspension and transported to the overbank during moderate to significant flooding. However, fine sand fractions in most rivers are transported as a suspension load during the flood [53,56]. The rivers transport sediments into oxbow lakes during short flooding periods; oxbow lakes develop distinctly between floods under more stable lacustrine environmental conditions. The flood events are documented in preserved sediments [57]. This is supported by the identified lithofacies (Table 1), where the overbank facies-dominated phase (OB1–OB5) is associated with a higher abundance of the EM4; the EM4 was dominated by the intensity and transported by river flood currents, with the increase in the proportion of EM4 with lower MS values (Figure 6) reflecting increasing flood strength and vice versa. Mechanisms by which sediments can be deposited during overbank flow are a function of grain size and sediment amount [58–60]; the coarse sediments are deposited in the channel proximity and transported by traction currents, in this case as graded suspensions [61], while the finer sediments are deposited at a distance as quiet water sedimentation as uniform suspensions [60,61]. The silt fractions of the EM4 are therefore considered to be deposited as distal overbank where the positive correlation EM3 showed a marginal correlation with other endmembers and the coarser percentile (D95) (Figure 7), indicating that EM3 is not sensitive to intensity changes in sedimentation processes during the lake filling; however, it could represent the distal overbank deposits. The indication of EM4 as a flood indicator is supported by its positive correlation with OM; the high carbon content can result from the deposition of carbon-rich sediments during floods [62]; however, fine sediments with high OM can be attributed to the low and continuous sedimentation at a distance from rivers [63]. Comparing the coarse-grained components (EM4) of the Tövises bed core with the NGRIP $\delta^{18}\text{O}$, annual precipitations, and mean annual precipitation records since 8000 BP, it is found that the EM4 records several cold and warm events during the relatively warmer early Holocene and the cooler late Holocene (Figure 8). Warm events with high precipitation are about circa 7500, 6000, 4700, 4000, 3600, 3000, 2500, 1400 and 700 BP. The warm event of the late Holocene was in 2000 BP, a cooler event with high precipitation was in 1700, and a cooler event with low precipitation was around 300 BP. The fluctuations are recorded at circa 7300–6700, 6000–4800, and 2700–1500 BP.

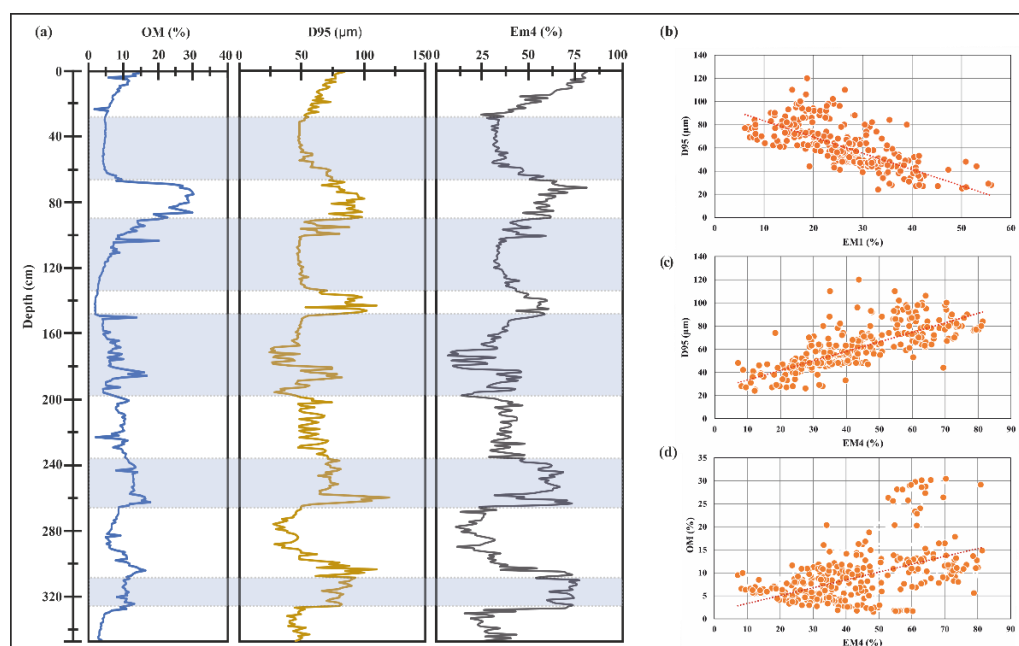


Figure 7. Sedimentary characteristics of the Tövises bed core. (a) OM, D95, and EM4 (b,c) linear correlations of D95 with EM1 and EM4, respectively. (d) Linear correlations of D95 with OM and EM4.

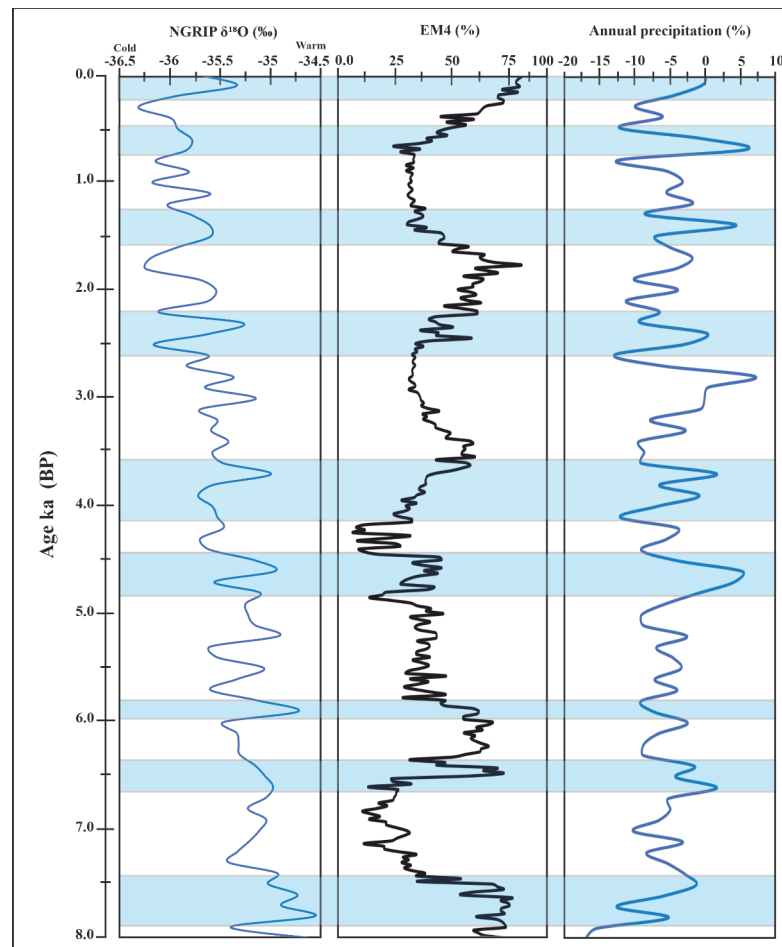


Figure 8. Comparison of the coarse grain-size endmembers (EM4) of Tövises bed core with annual mean precipitation as simulated by CCSM3 in TRaCE21ka experiment, averaged for “Europe” domain in Paleoview in Europe [64] and the NGRIP $\delta^{18}\text{O}$ [65] of the last 8000 BP.

5. Conclusions

The endmember modeling reveals invaluable insight into the alluviation history of the abandoned channel. Based on paleoenvironmental proxy indicators such as the change of grain-size endmembers, LOI, and MS, this study showed:

1. The age–depth model indicates that the core sequence represents sediment accumulation since 8000 BP. The grain-size composition, lithofacies, LOI, and MS reveal varying climatic conditions of wet and dry periods; the Tövises bed paleochannel evolved through an early lacustrine phase (oxbow lake) gradually infilled by lacustrine gyttjas, interbedded with wetland histosol, and periodically accumulated flood deposits.
2. The parameterized endmember modeling resulted in four endmembers (EM1–4), indicating different sedimentation conditions: EM1 is clay to very fine silt component of the oxbow lake filling, representing the lacustrine phase. EM2 and EM3 represent the intermediate component representing mainly silt transported resulting from a moderate flood; EM4 is a fraction of material transported during a significant flood when the river discharge was relatively high; it represents the overbank deposition phase.
3. This study demonstrates that partitioning the grain-size distribution of abandoned channel sediments into statistically robust grain-size endmembers provides various quantitative proxies that help to model the complex paleoenvironmental changes and climate history in the region during the Holocene.

Author Contributions: Conceptualization and methodology, A.E., D.M., J.G. and P.S.; validation, A.E. and J.G.; formal analysis, A.E.; age–depth model construction, D.M. and L.M.; data curation, writing—original draft preparation, A.E.; writing—review and editing, A.E. and J.G.; visualization; supervision, project administration, and funding acquisition, D.M. and P.S. All authors have read and agreed to the published version of the manuscript.

Funding: This research was sponsored by the Hungarian Government, Ministry of Human Capacities (20391-3/2018/FEKUSTRAT), European Regional Development Fund: GINOP-2.3.2-15-2016-00009 ‘ICER’ and Hungarian National Excellence Programme: NTP-NFTÖ-19-B-0158.

Data Availability Statement: The data presented in this study are available on request from the corresponding author. The data are not publicly available since the data will also be used in ongoing research.

Conflicts of Interest: The authors declare that there are no known competing financial interests or personal relationships that could have appeared to influence the work presented in this paper.

References

1. Shen, Z.; Aeschliman, M.; Conway, N. Paleodischarge reconstruction using oxbow lake sediments complicated by shifting hydrological connectivity. *Quat. Int.* **2021**, *604*, 75–81. [[CrossRef](#)]
2. Toonen, W.H.J.; Kleinhans, M.G.; Cohen, K.M. Sedimentary architecture of abandoned channel fills. *Earth Surf. Process. Landf.* **2012**, *37*, 459–472. [[CrossRef](#)]
3. Collinson, J.D.; Lewin, J. Alluvial cutoofs in Wales and the Borderlands. In *Modern and Ancient Fluvial Systems*; John Wiley & Sons, Inc.: Hoboken, NJ, USA, 1983.
4. Hooke, J.M. River channel adjustment to meander cutoffs on the River Bollin and River Dane, northwest England. *Geomorphology* **1995**, *14*, 235–253. [[CrossRef](#)]
5. Constantine, J.A.; Dunne, T.; Piégay, H.; Mathias Kondolf, G. Controls on the alluviation of oxbow lakes by bed-material load along the Sacramento river, California. *Sedimentology* **2010**, *57*, 389–407. [[CrossRef](#)]
6. Sun, D.; Bloemendal, J.; Rea, D.K.; Vandenberghe, J.; Jiang, F.; An, Z.; Su, R. Grain-size distribution function of polymodal sediments in hydraulic and aeolian environments, and numerical partitioning of the sedimentary components. *Sediment. Geol.* **2002**, *152*, 263–277. [[CrossRef](#)]
7. Shang, Y.; Beets, C.J.; Tang, H.; Prins, M.A.; Lahaye, Y.; van Elsas, R.; Sukselainen, L.; Kaakinen, A. Variations in the provenance of the late Neogene Red Clay deposits in northern China. *Earth Planet. Sci. Lett.* **2016**, *439*, 88–100. [[CrossRef](#)]
8. Liang, X.; Niu, Q.; Qu, J.; Liu, B.; Liu, B.; Zhai, X.; Niu, B. Applying end-member modeling to extricate the sedimentary environment of yardang strata in the Dunhuang Yardang National Geopark, northwestern China. *Catena* **2018**, *180*, 238–251. [[CrossRef](#)]
9. Kong, F.; Xu, S.; Han, M.; Chen, H.; Miao, X.; Kong, X.; Jia, G. Application of grain size endmember analysis in the study of dust accumulation processes: A case study of loess in Shandong Province, East China. *Sediment. Geol.* **2021**, *416*, 105868. [[CrossRef](#)]
10. Meyer, I.; Van Daele, M.; Tanghe, N.; De Batist, M.; Verschuren, D. Reconstructing East African monsoon variability from grain-size distributions: End-member modeling and source attribution of diatom-rich sediments from Lake Chala. *Quat. Sci. Rev.* **2020**, *247*, 106574. [[CrossRef](#)]
11. Li, T.; Li, T.J. Sediment transport processes in the Pearl River Estuary as revealed by grain-size end-member modeling and sediment trend analysis. *Geo-Mar. Lett.* **2018**, *38*, 167–178. [[CrossRef](#)]
12. Ha, H.J.; Chang, T.S.; Ha, H.K. Using end-member analysis to determine sediment dispersal and depositional processes on the Heuksan mud belt, southwest Korean shelf. *Geo-Mar. Lett.* **2021**, *41*, 1–13. [[CrossRef](#)]
13. de Mahiques, M.M.; Goya, S.C.; de Oliveira, R.A.; Kim, B.S.; de Lima Ferreira, P.A.; Figueira, R.C.; Bicego, M.C. Grain-size end-members and environmentally sensitive grain-size components: A comparative study in the mud shelf depocenters off southern Brazil. *Int. J. Sediment Res.* **2021**, *36*, 317–327. [[CrossRef](#)]
14. Huang, Y.; Xiao, J.; Xiang, R.; Liu, S.; Khokiattiwong, S.; Kornkanitnan, N.; Fan, J.; Wen, R.; Zhang, S.; Liu, J. Holocene Indian Summer Monsoon variations inferred from end-member modeling of sediment grain size in the Andaman Sea. *Quat. Int.* **2020**, *558*, 28–38. [[CrossRef](#)]
15. Vandenberghe, J.; Sun, Y.; Wang, X.; Abels, H.A.; Liu, X. Grain-size characterization of reworked fine-grained aeolian deposits. *Earth-Sci. Rev.* **2018**, *177*, 43–52. [[CrossRef](#)]
16. Zhang, X.; Zhang, H.; Chang, F.; Xie, P.; Li, H.; Wu, H.; Ouyang, C.; Liu, F.; Peng, W.; Zhang, Y. Long-range transport of aeolian deposits during the last 32 kyr inferred from rare earth elements and grain-size analysis of sediments from Lake Lugu, Southwestern China. *Palaeogeogr. Palaeoclimatol. Palaeoecol.* **2021**, *567*, 110248. [[CrossRef](#)]
17. Ijmker, J.; Stauch, G.; Dietze, E.; Hartmann, K.; Diekmann, B.; Lockot, G.; Opitz, S.; Wünnemann, B.; Lehmkuhl, F. Characterisation of transport processes and sedimentary deposits by statistical end-member mixing analysis of terrestrial sediments in the Donggi Cona lake catchment, NE Tibetan Plateau. *Sediment. Geol.* **2012**, *281*, 166–179. [[CrossRef](#)]

18. Dietze, E.; Diekmann, B.; Opitz, S.; Hartmann, K. Quantifying depositional processes in sediment archives using end-member modelling of grain size data. In Proceedings of the EGU General Assembly Conference Abstracts, Vienna, Austria, 7–12 April 2013.
19. Dietze, E.; Maussion, F.; Ahlborn, M.; Diekmann, B.; Hartmann, K.; Henkel, K.; Kasper, T.; Lockot, G.; Opitz, S.; Haberzettl, T. Sediment transport processes across the Tibetan Plateau inferred from robust grain-size end members in lake sediments. *Clim. Past* **2014**, *10*, 91–106. [[CrossRef](#)]
20. Wang, J.; He, Z.; Li, L. Palaeoseismic records in lacustrine sediments—A case study of the Daqingshan piedmont fault and Hasuhai Lake in Inner Mongolia, China. *Basin Res.* **2021**, *33*, 681–704. [[CrossRef](#)]
21. Toonen, W.H.J.; Winkels, T.G.; Cohen, K.M.; Prins, M.A.; Middelkoop, H. Lower Rhine historical flood magnitudes of the last 450 years reproduced from grain-size measurements of flood deposits using End Member Modelling. *Catena* **2015**, *130*, 69–81. [[CrossRef](#)]
22. Pang, H.; Li, F.; Gao, H.; Jia, Y.; Chen, D.; Zhang, X. Application of Hierarchical Clustering Endmember Modeling Analysis for Identification of Sedimentary Environment in the Houtao Section of the Upper Yellow River. *Water* **2022**, *14*, 1025. [[CrossRef](#)]
23. Weltje, G.J. End-member modeling of compositional data: Numerical-statistical algorithms for solving the explicit mixing problem. *Math. Geol.* **1997**, *29*, 503–549. [[CrossRef](#)]
24. Dietze, E.; Hartmann, K.; Diekmann, B.; Ijmker, J.; Lehmkuhl, F.; Opitz, S.; Stauch, G.; Wünnemann, B.; Borchers, A. An end-member algorithm for deciphering modern detrital processes from lake sediments of Lake Donggi Cona, NE Tibetan Plateau, China. *Sediment. Geol.* **2012**, *243–244*, 169–180. [[CrossRef](#)]
25. Paterson, G.A.; Heslop, D. New methods for unmixing sediment grain size data. *Geochem. Geophys. Geosystems* **2015**, *15*, 4494–4506. [[CrossRef](#)]
26. Yu, S.Y.; Colman, S.M.; Li, L. BEMMA: A Hierarchical Bayesian End-Member Modeling Analysis of Sediment Grain-Size Distributions. *Math. Geosci.* **2016**, *48*, 723–741. [[CrossRef](#)]
27. Zhang, X.; Wang, H.; Xu, S.; Yang, Z. A basic end-member model algorithm for grain-size data of marine sediments. *Estuar. Coast. Shelf Sci.* **2020**, *236*, 106656. [[CrossRef](#)]
28. Vincze, I.; Finsinger, W.; Jakab, G.; Braun, M.; Vincze, I.; Finsinger, W.; Jakab, G.; Braun, M.; Hubay, K. Paleoclimate reconstruction and mire development in the Eastern Great Hungarian Plain for the last 20,000 years To cite this version: HAL Id: Hal-02279803. *Rev. Palaeobot. Palynol.* **2020**, *271*, 104112. [[CrossRef](#)]
29. Kiss, T.; Hernesz, P.; Sümeghy, B.; Györgyövícs, K.; Sipos, G. The evolution of the Great Hungarian Plain fluvial system e Fluvial processes in a subsiding area from the beginning of the Weichselian. *Quat. Int.* **2015**, *388*, 142–155. [[CrossRef](#)]
30. Kustár, R.; Molnár, D.; Sümegi, P.; Töröcsik, T.; Sávai, S. Preliminary paleoecological reconstruction of long-term relationship between human and environment in the northern part of Danube-along Plain, Hungary. *Open Geosci.* **2016**, *8*, 405–419. [[CrossRef](#)]
31. Sümegi, P.; Molnár, M.; Jakab, G.; Persaits, G.; Majkut, P.; Páll, D.G.; Gulyás, S.; Jull, A.T.; Töröcsik, T. Radiocarbon-Dated Paleoenvironmental Changes on a Lake and Peat Sediment Sequence from the Central Great Hungarian Plain (Central Europe) During the last 25,000 years. *Radiocarbon* **2011**, *53*, 85–97. [[CrossRef](#)]
32. Szőőr, G.; Sümegi, P.; Balázs, É. Sedimentological and geochemical facies analysis Upper Pleistocene fossil soil zones discovered in the Hajdúság region, NE Hungary. *Quat. Environ. Hung. Stud. Geogr. Hung.* **1991**, *26*, 47–59.
33. Sümegi, P.; Vissi, E. A pocsaji láp kialakulása és fejlődéstörténete. *Calandrella* **1991**, *5*, 15–27.
34. Konert, M.; Vandenbergh, J. Comparison of laser grain size with pipette and sieve analysis: A solution for the underestimation of the clay fraction. *Sedimentology* **1997**, *44*, 523–535. [[CrossRef](#)]
35. Blaauw, M.; Christeny, J.A. Flexible paleoclimate age-depth models using an autoregressive gamma process. *Bayesian Anal.* **2011**, *6*, 457–474. [[CrossRef](#)]
36. Wentworth, C.K. A Scale of Grade and Class Terms for Clastic Sediments. *J. Geol.* **1922**, *30*, 377–392. [[CrossRef](#)]
37. Wu, L.; Krijgsman, W.; Liu, J.; Li, C.; Wang, R.; Xiao, W. CFLab: A MATLAB GUI program for decomposing sediment grain size distribution using Weibull functions. *Sediment. Geol.* **2020**, *398*, 105590. [[CrossRef](#)]
38. Santisteban, J.I.; Mediavilla, R.; López-Pamo, E.; Dabrio, C.J.; Zapata, M.B.R.; García, M.J.G.; Castaño, S.; Martínez-Alfaro, P.E. Loss on ignition: A qualitative or quantitative method for organic matter and carbonate mineral content in sediments? *J. Paleolimnol.* **2004**, *32*, 287–299. [[CrossRef](#)]
39. Vereş, D. A Comparative Study Between Loss on Ignition and Total Carbon Analysis on Mineralogenic Sediments. *Stud. Univ. Babeş-Bolyai Geol.* **2002**, *47*, 171–182. [[CrossRef](#)]
40. Dearing, J. *John Dearing Environmental Magnetic Susceptibility Using the Bartington MS2 System*; Bartington Instruments Ltd.: Witney, UK, 1999.
41. Scouse, R.A. *Introduction to Statistical Quality Control*; John Wiley & Sons: Hoboken, NJ, USA, 1985; Volume 10, ISBN 9780470169926.
42. Hicks, J.L.; Evans, J.E. Oxbow Lakes as Geological Archives of Historical Changes in Channel Substrate, Swan Creek, Toledo, Ohio (USA). *Open J. Mod. Hydrol.* **2022**, *12*, 32–54. [[CrossRef](#)]
43. Folk, R.L. The Distinction between Grain Size and Mineral Composition in Sedimentary-Rock Nomenclature. *J. Geol.* **1954**, *62*, 344–359. [[CrossRef](#)]
44. Syvitski, J.P.M.; Vorosmarty, C.J.; Kettner, A.J.; Green, P. Impact of humans on the flux of terrestrial sediment to the global coastal ocean. *Science* **2005**, *308*, 76–80. [[CrossRef](#)]
45. Tooth, S. Dryland Fluvial Environments: Assessing Distinctiveness and Diversity from a Global Perspective. In *Treatise on Geomorphology*; Shroder, J.F., Ed.; Academic Press: San Diego, CA, USA, 2013; pp. 612–644, ISBN 978-0-08-088522-3.

46. Juez, C.; Hassan, M.A.; Franca, M.J. The Origin of Fine Sediment Determines the Observations of Suspended Sediment Fluxes Under Unsteady Flow Conditions. *Water Resour. Res.* **2018**, *54*, 5654–5669. [[CrossRef](#)]
47. Pannatier, E.G. Sediment Accumulation and Historical Deposition of Trace Metals and Trace Organic Compounds in the Mackenzie Delta (Northwest Territories, Canada). Ph.D. Thesis, University of Geneva, Geneva, Switzerland, 1997, ISBN 2-940153-09-4.
48. Davis, B.A.S.; Brewer, S.; Stevenson, A.C.; Guiot, J.; Allen, J.; Almquist-Jacobson, H.; Ammann, B.; Andreev, A.A.; Argant, J.; Atanassova, J.; et al. The temperature of Europe during the Holocene reconstructed from pollen data. *Quat. Sci. Rev.* **2003**, *22*, 1701–1716. [[CrossRef](#)]
49. Perşoiu, A.; Onac, B.P.; Wynn, J.G.; Blaauw, M.; Ionita, M.; Hansson, M. Holocene winter climate variability in Central and Eastern Europe. *Sci. Rep.* **2017**, *7*, 1–8.
50. Moore, P.D. The ecology of peat-forming processes: A review. *Int. J. Coal Geol.* **1989**, *12*, 89–103. [[CrossRef](#)]
51. Marsh, P. Permafrost and lakes in the Mackenzie Delta. *Collect. Nord.* **1990**, *54*, 131–136.
52. Gorsline, D.S. Introduction to a symposium on fine-grained sedimentology. *Geo-Mar. Lett.* **1984**, *4*, 133–138. [[CrossRef](#)]
53. Thompson, R.; Oldfield, F. *Environmental Magnetism*; Springer: Berlin/Heidelberg, Germany, 1986; Volume 7, ISBN 9772081415.
54. Tite, M.S.; Linington, R.E. Effect of climate on the magnetic susceptibility of soils. *Nature* **1975**, *256*, 565–566. [[CrossRef](#)]
55. Mullins, C.E. Magnetic Susceptibility of The Soil And Its Significance In Soil Science—A Review. *J. Soil Sci.* **1977**, *28*, 223–246. [[CrossRef](#)]
56. Brownlie, W.R.; Taylor, B.D. *Coastal Sediment Delivery by Major Rivers in Southern California*; EQL Report No. L7-C; Environmental Quality Laboratory: Pasadena, CA, USA, 1981.
57. Gasiowski, M.; Hercman, H. Recent changes of sedimentation rate in three Vistula oxbow lakes determined by 210 Pb dating. *Geochronometria* **2005**, *24*, 33–39.
58. Pizzuto, J.E. Sediment diffusion during overbank flows. *Sedimentology* **1987**, *34*, 301–317. [[CrossRef](#)]
59. Knighton, D. *Fluvial Forms and Processes: A New Perspective*, 2nd ed.; Routledge: London, UK, 1998.
60. Pierce, A.R.; King, S.L. Spatial dynamics of overbank sedimentation in floodplain systems. *Geomorphology* **2008**, *100*, 256–268. [[CrossRef](#)]
61. Eltjani, A.; Molnár, D.; Makó, L.; Geiger, J.; Sümegi, P. Applying Grain-Size and Compositional Data Analysis for Interpretation of the quaternary oxbow lake sedimentation processes: Great hungarian plain. *Stud. Quat.* **2022**, *39*.
62. Pinay, G.; Fabre, A.; Vervier, P.; Gazelle, F. Control of C, N, P distribution in soils of riparian forests. *Landsc. Ecol.* **1992**, *6*, 121–132. [[CrossRef](#)]
63. Cierjacks, A.; Kleinschmit, B.; Kowarik, I.; Graf, M.; Lang, F. Organic matter distribution in floodplains can be predicted using spatial and vegetation structure data. *River Res. Appl.* **2011**, *27*, 1048–1057. [[CrossRef](#)]
64. Fordham, D.A.; Saltré, F.; Haythorne, S.; Wigley, T.M.L.; Otto-Bliesner, B.L.; Chan, K.C.; Brook, B.W. PaleoView: A tool for generating continuous climate projections spanning the last 21,000 years at regional and global scales. *Ecography* **2017**, *40*, 1348–1358. [[CrossRef](#)]
65. North Greenland Ice Core Project members. High-resolution record of Northern Hemisphere climate extending into the last interglacial period. *Nature* **2004**, *431*, 147–151. [[CrossRef](#)]